

Review

Multifunctional Upconversion-Magnetic Hybrid Nanostructured Materials: Synthesis and Bioapplications

Xiaomin Li, Dongyuan Zhao and Fan Zhang✉

Department of Chemistry and Laboratory of Advanced Materials, Fudan University, Shanghai, China.

✉ Corresponding author: Email: zhang_fan@fudan.edu.cn

© Ivyspring International Publisher. This is an open-access article distributed under the terms of the Creative Commons License (<http://creativecommons.org/licenses/by-nc-nd/3.0/>). Reproduction is permitted for personal, noncommercial use, provided that the article is in whole, unmodified, and properly cited.

Received: 2012.09.04; Accepted: 2012.10.24; Published: 2013.03.21

Abstract

The combination of nanotechnology and biology has developed into an emerging research area: nano-biotechnology. Upconversion nanoparticles (UCNPs) have attracted a great deal of attention in bioapplications due to their high chemical stability, low toxicity, and high signal-to-noise ratio. Magnetic nanoparticles (MNPs) are also well-established nanomaterials that offer controlled size, ability to be manipulated externally, and enhancement of contrast in magnetic resonance imaging (MRI). As a result, these nanoparticles could have many applications in biology and medicine, including protein purification, drug delivery, and medical imaging. Because of the potential benefits of multimodal functionality in biomedical applications, researchers would like to design and fabricate multifunctional upconversion-magnetic hybrid nanostructured materials. The hybrid nanostructures, which combine UCNPs with MNPs, exhibit upconversion fluorescence alongside superparamagnetism property. Such structures could provide a platform for enhanced bioimaging and controlled drug delivery. We expect that the combination of unique structural characteristics and integrated functions of multifunctional upconversion-magnetic nanoparticles will attract increasing research interest and could lead to new opportunities in nano-bioapplications.

Key words: Upconversion nanoparticles, Magnetic nanoparticles

1. Introduction

Photon upconversion (UC) is capable of absorbing near infrared (NIR) radiation, and emission radiation of UV or visible light. The UC process proceeds by different mechanisms, which are summarized and discussed in detail in several review articles [1–5] and can be roughly divided into three classes: energy transfer upconversion (ETU) [6], excited-state absorption (ESA), and photon avalanche (PA) [7]. In past few years, UC fluorescent materials have attracted a great deal of attention due to their attractive merits involving narrow emission peaks, large anti-stokes shifts, and low toxicity [8–18]. Upconversion nanoparticles (UCNPs), which are able to emit visible or UV photons under excitation by near-infrared light, have been found many potential applications in different

fields, such as solid-state lasers, three-dimensional flat-panel displays, solar cells, and especially bio-labels and bio-imaging. Compared with traditional fluorescence imaging using organic dyes or quantum dots, the NIR-light-excited UC luminescence imaging relying on lanthanide-doped rare-earth UCNPs exhibits improved tissue penetration depth, higher photochemical stability, and free of auto-fluorescence [8–18]. According to the selection of the host materials, the UC materials can be classified into two parts, one kind is based on metal oxide materials (LuPO_4 , YVO_4 , Y_2O_3 etc.), the other kind is based on fluorides [LnF_3 , $\text{M}(\text{RE})\text{F}_4$ ($\text{M}=\text{Li}$, Na , K ; $\text{RE}=\text{Rare Earth}$) etc.]. So far, a variety of chemical techniques, have been developed to synthesize lan-

thanide-doped UC nanocrystals [19-30], such as co-precipitation method, thermal decomposition, hydrothermal (solvothermal) synthesis, sol-gel processing and combustion synthesis, and so on. As a new generation luminescent materials, rare-earth UCNPs have been considered to be an excellent luminescent probes for bio-imaging, which include tumor-targeted imaging, lymphatic imaging, vascular imaging, cell tracking and so on.

In the past two decades, the synthetic iron oxide magnetic nanoparticles (MNPs) and related nanoparticles have played an important role in many bio-application fields [31-37]. Some forms of these nanoparticles are now clinically used for improving magnetic resonance (MR) contrast and have also been used in magnetic targeting drugs delivery system. Furthermore, the rapid development in the synthetic methods for preparing MNPs have allowed researchers to synthetically control the important features of these probes, such as size, magnetic dopants, magneto-crystalline phases, and surface states, resulting in the discovery of "designed" MNPs. These innovative nanoparticle probes exhibit superior magnetism and MR contrast effects which have been shown to be better than that of conventional MR contrast agents [38-41]. According to the composition of the MNPs, they can be classified into three major types: single metal oxide (iron oxide, manganese oxide, cobalt oxide *etc.*), dopant MNPs [MFe_2O_4 , $M = Mn, Ni, Co$], metal-Alloy (FeCo, FePt, *etc.*). MNPs High-quality synthetic MNPs are typically prepared through the thermal decomposition of metal-complex precursors in hot non-hydrolytic organic solution containing surfactants. Thermal decomposition of the precursors generates monomers and their aggregation above a supersaturation level induces nucleation and subsequent nanoparticles growth [42-50]. During these stages, by tuning growth parameters, such as monomer concentration, crystalline phase of the nuclei, choice of solvent and surfactants, growth temperature and time, and surface energy, it is possible to control the size, composition, and magneto-crystalline phase of MNPs.

The rapid development in nanotechnology has allowed the engineering of various functional nanomaterials with multiple discrete function-related components integrated in one nanoparticle for applications in multimodality bio-applications to circumvent the limitations of each single mode application. Conventional chemotherapy is commonly used in the clinical management of many cancers, often with severe side effects due to the cytotoxicity of the agents and the genetic heterogeneity of the tumors, that is, their phenotypic drug sensitivity or resistivity [51].

Nano-engineered drug-delivery systems could improve the clinical performance of conventional chemotherapeutic agents and reduce overall toxicity by enhancing the specificity of the drug's delivery through tumor targeting and making elevated local dosages possible [52-54]. A major goal in nano-medicine is the coherent implementation of multifunctional platforms within a single targeted nano-delivery system that would simultaneously perform diagnosis, targeted delivery and efficient therapy (theranostics) [55-60]. Along these lines, luminescent and magnetic nanoparticles have been used as bio-labeling, contrast agents, and for magnetic resonance imaging (MRI) and targeted drug delivery, leading recently to major advances in bio-applications [55-60]. Until recently, the multifunctional luminescent-magnetic materials have been based on quantum dots, organic molecules, and polymers [55-57]. The biological applications of these down-conversion luminescent materials have at times been restricted due to their limited tissue-penetration depth, low signal-to-background ratio given the significant auto-fluorescence from biological tissues, in some cases by chemical instability, and by uncertain toxicity [61]. An alternative that avoids some of these limitations is near-infrared to UV-vis UCNPs. Here the luminescent materials emit visible light upon NIR-light excitation making them superior bio-imaging agents than systems employing down-conversion luminescent materials. While not wholly free from tissue-penetration limits, UC materials absorbing at NIR wavelengths greatly improve penetration depth relative to down-conversion materials, thereby also decreasing photo-damage to tissue especially at high light fluxes. UC materials also typically exhibit high photo and chemical stability allowing long integration times to be used and increasing signal-to-noise due to an essentially dark UC background [62-65]. On the other hand, to benefit from its magnetic properties, the magnetic materials can serve as agent of the MRI and targeted drug delivery. So, with the upconversion-magnetic hybrid nanostructured materials, we will certainly accomplish multimodality bio-applications to circumvent the limitations of each single mode application.

In this review, we describe some potentially useful designs and applications of multifunctional upconversion luminescent-magnetic nanoparticles for bio-applications, which have been attracting increased research effort because of their easily accessible multimodality. The integration of UCNPs and MNPs forms multi-functional structures with both fluorescent and magnetic properties, which lead to the demonstration of intracellular manipulation of na-

nanoparticles and a promising candidate for dual-functional molecular imaging (i.e. combining MRI and fluorescence imaging). Furthermore, the multi-functional nanomaterials emit visible luminescence upon NIR excitation can be manipulated using an external magnetic field, for example, as a contrast agent for a specific target, making them attractive for a variety of biological applications. For example, we can use them in *in vitro* drug release assays and *in vivo* anti-tumor agents.

2. Synthesis and Properties of the Multi-functional Upconversion-Magnetic Nanoparticles

Generally, there are three kinds of strategies to fabricate multifunctional upconversion-magnetic nanoparticles. The first strategy is SiO₂ assisted synthesis of the upconversion-magnetic multifunctional nanoparticles [66-70]. The second approach is based on combining UCNPs and magnetic nanocrystals assisted by cross-linker [71-74]. The third way is based on the seed-mediated growth method [75-77].

2.1 SiO₂ assisted synthesis of upconversion-magnetic multifunctional nanoparticles

Silanization is a popular technique for surface modification of nanoparticles since silica is highly biocompatible, ease of surface modification, which would allow for biolabeling, drug targeting, and delivery. Furthermore, the SiO₂-coated functional nanoparticles can be protected by the SiO₂ shell to against the influence of physiological condition and outside environments, which will show more stable properties. So, with assistance of the advantages of the SiO₂, SiO₂ assisted method is considered to be one of the most effective route to synthesize the upconversion-magnetic multifunctional nanoparticles.

Most recently, Zhang and co-workers fabricated nanorattles consisting of hydrophilic rare-earth doped NaYF₄ shells each containing a loose magnetic nanoparticle through an ion-exchange process (Figure 1) [66]. The inner magnetic Fe₃O₄ nanoparticles are coated with a SiO₂ layer to avoid iron leaching in acidic biological environments. This multi-functional mesoporous nanostructure with both UC luminescent and magnetic properties has excellent water dispersibility and a high drug-loading capacity. As shown in Figure 2, The Fe₃O₄@SiO₂ nanoparticles were synthe-

sized from monodispersed ~20 nm diameter Fe₃O₄ nanocrystals as a core, using a reverse-microemulsion method. The Fe₃O₄@SiO₂ nanospheres are then coated with a layer of Y/Yb, Er(OH)CO₃.H₂O via a homogeneous precipitation method. Thermal treatment at high temperature transformed the amorphous Y/Yb, Er(OH)CO₃.H₂O into the cubic phase of Y₂O₃. The Fe₃O₄@SiO₂@ α -NaYF₄/Yb,Er magnetic upconversion fluoride nanorattles (MUC-F-NR) are formed via ion-exchange of MUC-O-NS in the presence of HF and NaF solution. Finally, mesoporous multifunctional UC luminescent and magnetic "nanorattle" was obtained. The nanorattles emit visible luminescence upon NIR excitation and have very good superparamagnetic property, making it an attractive system for a variety of biological applications. Furthermore, the BET surface area and the pore size are calculated to be ~73 m²/g and 4.8 nm, which offers possibilities for further magnetic targeted drug delivery. This method could also extend to the synthesis of core/shell Fe₃O₄@NaLuF₄:Yb,Er/Tm nanostructure.

Hu et al. presents a facile method for the fabrication of core-shell-structured NaYF₄:Yb,Er/Tm@SiO₂@Fe₃O₄ nanoparticles (Figure 2) [70]. In this approach, when the EDTA-capped NaYF₄:Yb,Er/Tm nanoparticles were mixed with the oleic acid-modified magnetic Fe₃O₄ nanoparticles in isopropyl alcohol, followed by addition of TEOS and ammonium hydroxide, core shell NaYF₄:Yb,Er/Tm@SiO₂@Fe₃O₄ nanoparticles were directly yielded; neither surface modification nor high temperature was needed. The obtained nanoparticles have very good superparamagnetic and luminescent properties.

Liu et al. have also reported a new type of monodisperse core/shell nanoparticles with both UC fluorescent nanocrystals and superparamagnetic (SPM) nanocrystals encapsulated in silica shells (SiO₂/UC-SPM) (Figure 3) [68]. The obtained composite nanoparticles are capable of emitting pure eye-visible fluorescence upon NIR excitation and being driven by an external magnetic field to a specific target, which make them attractive for a variety of biomedical applications, such as bioimaging, drug targeting and bio-separation. The synthesis method is based on the simple and more convenient one pot reverse-microemulsion method. However, owing to the lack of the mesoporous, it is limited in practical drug delivery system.

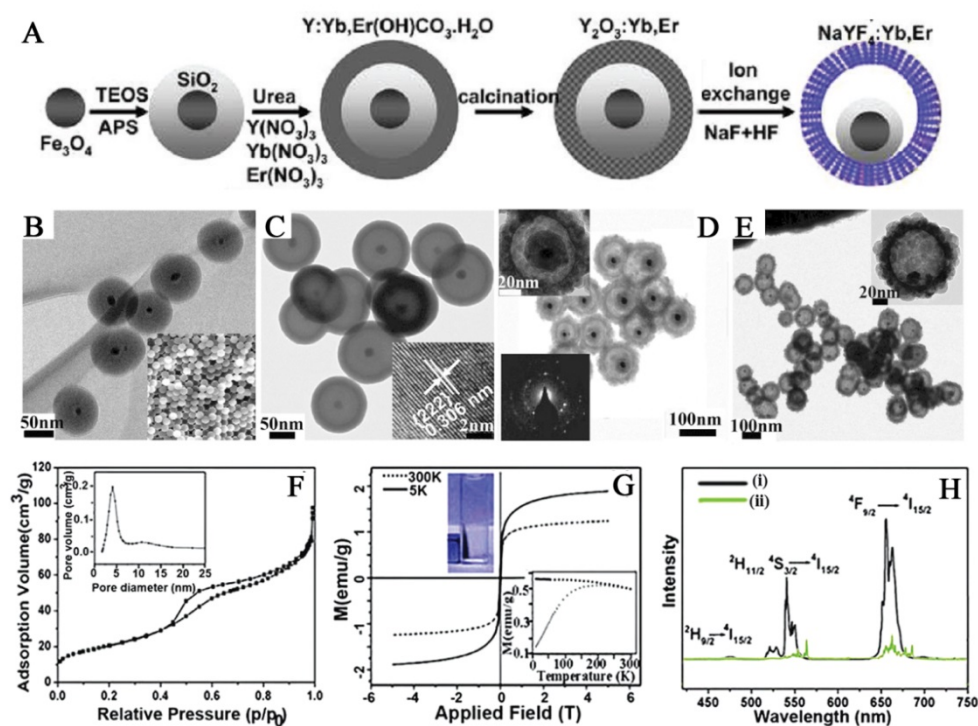


Figure 1. (A) Synthetic procedure for the drug-loaded $\text{Fe}_3\text{O}_4@SiO_2@ \alpha\text{-NaYF}_4/\text{Yb,Er}$ nanorattles (DOX-MUC-F-NR). (B) TEM and SEM images of $\text{Fe}_3\text{O}_4@SiO_2$ nanospheres. (C) TEM image of MUC-O-NS; inset is an HRTEM image after growing the outer $\text{Y}_2\text{O}_3/\text{Yb,Er}$ layer. (D) TEM image of the MUC-F-NR; insets are higher-magnification TEM image of one (upper left) and the SAED image recorded on part of the $\alpha\text{-NaYF}_4/\text{Yb,Er}$ shell (lower left). (E) TEM image of $\text{Fe}_3\text{O}_4@ \alpha\text{-NaYF}_4/\text{Yb,Er}$ with SiO_2 fully etched; inset is a higher-magnification TEM image of a single hollow nanosphere. (F) N_2 adsorption-desorption isotherms and pore diameter distribution of MUC-F-NR. (G) The magnetization of MUC-F-NR measured at 5 and 300 K; inset in lower right is the temperature dependence of ZFC and FC magnetization curve for the MUC-F-NR; inset in upper left shows that MUC-F-NR can be physically attracted by the applied magnetic field at room temperature in water. (H) UC spectra of MUC-F-NR (i) and MUC-O-NS (ii) upon excitation at 980 nm. This figure is reprinted from [66]. Copyright 2012 American Chemical Society.

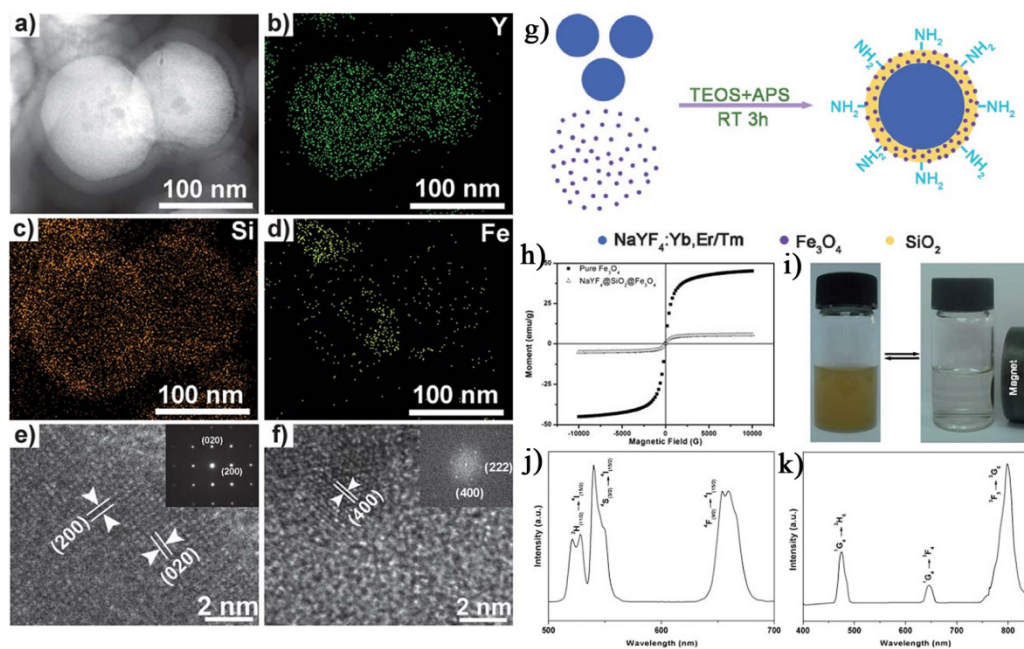


Figure 2. a) Bright-field TEM image and b–d) EDX elemental mappings of $\text{NaYF}_4:\text{Yb,Er}@SiO_2@Fe_3O_4$, e) HRTEM image of $\text{NaYF}_4:\text{Yb,Er}@SiO_2@Fe_3O_4$ (inset: SAED image of $\text{NaYF}_4:\text{Yb,Er}$) and f) HRTEM image of Fe_3O_4 (inset: FFT image of Fe_3O_4). g) Schematic illustration of the formation of $\text{NaYF}_4:\text{Yb,Er/Tm}@SiO_2@Fe_3O_4$ nanoparticles. h) The magnetic hysteresis loops for pure Fe_3O_4 and $\text{NaYF}_4:\text{Yb,Er}@SiO_2@Fe_3O_4$. i) The separation process of the $\text{NaYF}_4:\text{Yb,Er}@SiO_2@Fe_3O_4$ nanocomposite particles by a magnet. j, k) Room-temperature UC luminescent spectra of $\text{NaYF}_4:\text{Yb,Er}@SiO_2@Fe_3O_4$ nanoparticles and $\text{NaYF}_4:\text{Yb,Tm}@SiO_2@Fe_3O_4$ nanoparticles excited by 980 nm IR light. This figure is reprinted from [70]. Copyright 2011, Royal Society of Chemistry.

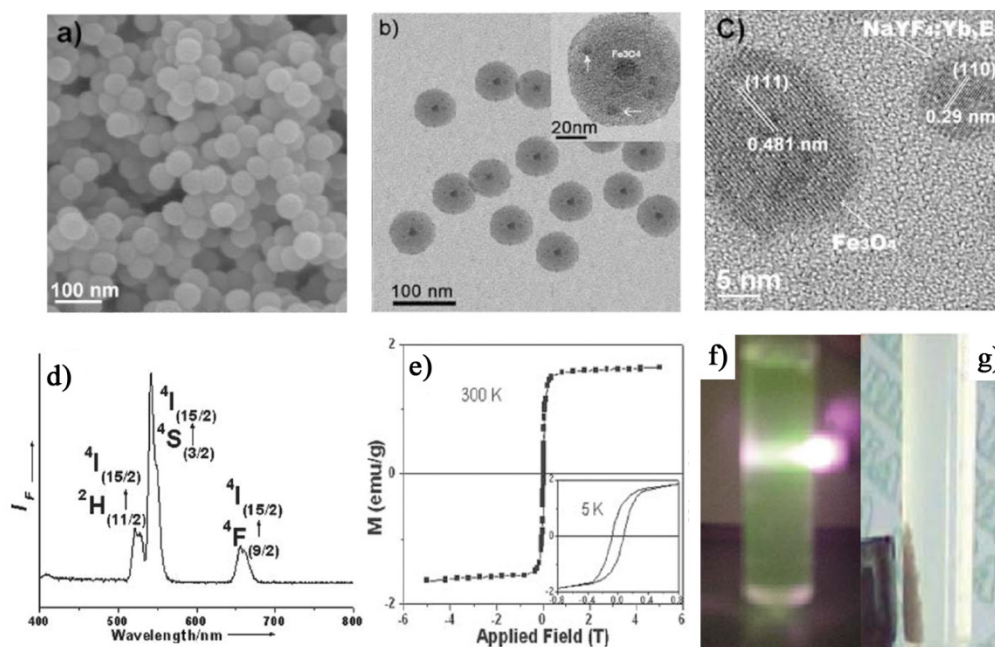


Figure 3. FE-SEM (a), TEM (b) and HRTEM (c) images of silica nanoparticles encapsulating UCNP and SPM nanocrystals. (d) Room-temperature up-conversion fluorescence spectra of $\text{SiO}_2/\text{UCNPs-SPM}$ nanoparticles under 980 nm NIR excitation. (e) Magnetic measurements of $\text{SiO}_2/\text{UCNPs-SPM}$ nanoparticles showing magnetization–applied magnetic field (M–H). The inset in (e) is a magnified view of the magnetization curves at low applied fields. (f, g) Photograph of the upconversion fluorescence (green) of $\text{SiO}_2/\text{UCNPs-SPM}$ nanoparticles in aqueous solutions and driven by an external magnet. This figure is reprinted from [68]. Copyright 2008, Royal Society of Chemistry.

2.2 Cross-linker assisted synthesis of upconversion-magnetic multifunctional nanoparticles

In addition to the SiO_2 assisted synthesis method, cross-linker assisted method has also been developed [71-74]. Cheng et al. describe a novel class of multifunctional nanoparticles (MFNPs) based on UCNP with combined optical and magnetic properties [71]. The MFNPs were prepared by layer-by-layer (LBL) self-assembly (Figure 4). Ultra small superparamagnetic dopamine (DA) modified iron oxide (Fe_3O_4) nanoparticles (IONPs) are adsorbed on the surface of Poly(acrylic acid) (PAA) modified NaYF_4 -based UCNP by electrostatic attraction to form a UCNP-IONP complex, on top of which a thin gold shell is formed by seed-induced reduction growth. The layer of IONPs between UCNP and the Au shell not only affords MFNPs magnetic properties but also significantly reduces the luminescence quenching effects of the gold nanostructure to UCNP. The primary force between the poly(acrylic acid) modified UCNP and dopamine modified magnetic particles is from the condensation reaction between the carboxyl and amino group.

Shen and co-workers reported the $\text{Fe}_3\text{O}_4/\text{NaYF}_4:\text{Yb,Er}$ hetero-NPs synthesized by a novel ligand anchoring strategy (Figure 5) [72]. Fe_3O_4

NPs are localized at the surface of UC NP assisted by cross linkers. Compared with other chemical linkage methods for hybrid nano-structures, this cross linker anchoring strategy comprises the ligand exchange process, crystallization of Fe_3O_4 NPs and integration into hetero-NPs in a sequential one-pot reaction. The process is facile and effective for construction of hetero-NPs in a solvo-thermal system. This approach is not limited by lattice mismatch for different functional components, and is applicable to QDs and noble metal NPs, etc. The hetero-NPs well preserve the UC luminescence and room-temperature superparamagnetism, which enables both effective optical detection and magnetic trapping. They could be fabricated into luminescent micro-patterns with magnetic manipulation.

Xu et al. demonstrate a facile synthetic method to prepare a novel nanocomposite for multi-modal imaging and imaging combined drug delivery (Figure 6) [74]. They can encapsulate hydrophobic UCNP together with iron oxide (IO) nanoparticles by using an amphiphilic block copolymer, poly(styrene-block-allyl alcohol) ($\text{PS}_{16}\text{-b-PAA}_{10}$), via a microemulsion method, obtaining an UC-IO@Polymer multi-functional nanocomposite system. By further introducing a fluorescent Squaraine (SQ) dye during sample preparation, the obtained UC-IO@Polymer-SQ could be used for triple-modal

UC luminescence/down-conversion FL/MR imaging in vitro and in vivo.

2.3 Seed-mediated growth method for the synthesis of upconversion-magnetic multifunctional nanoparticles

When considering seed-mediated growth, the energetics of the reaction plays an important role. The energy barrier for the homogeneous nucleation of a material is typically quite large; it is rare in nanoparticles systems that particles will spontaneously nucleate and grow in solution without a driving force such as a supersaturated solution, a strong reducing agent, or the use of high temperatures to overcome the energy barrier toward nucleation. Attempts to synthesize hybrid nanoparticles make use of this energy barrier, or perhaps more accurately the lower energy barrier for the heterogeneous nucleation of a second phase onto a seed particle. In comparison with the methods mentioned above, the seed-mediated growth method should be simpler, and show more stable hybrid nanostructure than the cross-linker assisted and SiO₂ assisted method. On the other hand, the size of the obtained core/shell hybrid nanostructure can be easily controlled below 100 nm or smaller, which will increase the biocompatibility of the materials. So we can extend this seed-mediated growth method to the synthesis of the upconversion-magnetic

multifunctional nanoparticles [75-77].

Xia et al. synthesized new core/shell structured NaYF₄:Yb³⁺,Tm³⁺@Fe_xO_y nanoparticles, with 20 nm Yb³⁺, Tm³⁺ co-doped NaYF₄ nanoparticles as a core and 5 nm Fe_xO_y nanoparticles as a shell [75]. These core/shell nanoparticles exhibit excellent near-infrared UC luminescence emission at 800 nm under excitation by a continuous-wave 980 nm laser and superparamagnetic properties with a saturation magnetization of ~12 emu/g (Figure 7).

Similarly, Zhong and co-workers introduced a core-shell structured NPs composed of magnetite core and up-conversion luminescent shell by using the seed-mediated growth method (Figure 8) [76]. Each of the components in the nanocomposites displays a unique function. Fe₃O₄ as the core endows nanoparticles with magnetic property, and the outer NaGdF₄:Yb/Er shell is to improve the luminescent efficiency. Although the composite obtained by using seed-mediated growth method gain the properties of both UC luminescence and magnetic properties, but to date, core/shell structures based on UC and magnetic nanoparticles have not been certified from direct measurements. So, more direct evidences should be provided on the characterizations of the obtained upconversion-magnetic multifunctional materials synthesized by this method in the future.

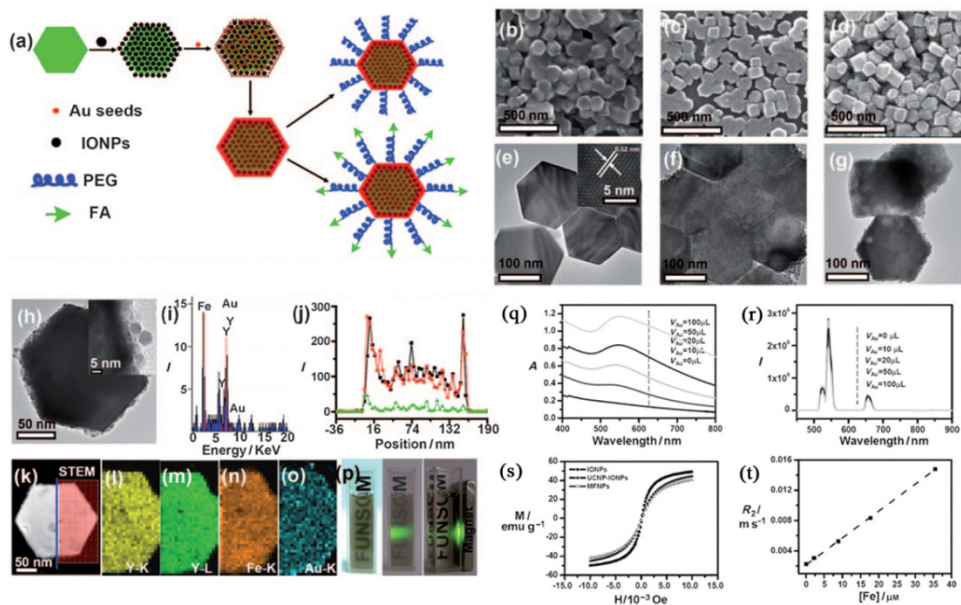


Figure 4. a) Strategy for MFNP synthesis and functionalization. b-d) SEM images of the UCNPs (b), UCNP-IONP nanocomposites (c), and UCNP-IONP-Au MFNPs (d). e-g) TEM images of UCNPs (e), the inset shows the HRTEM image of a MFNP and the indicated d spacing is 0.52 nm; UCNP-IONP nanocomposites (f); and MFNPs (g). h) A TEM image of a single MFNP with high magnification. Inset is a HRTEM image showing the edge of this MFNP. i) EDS of the MFNPs under the STEM pattern. j, k) A STEM image of a single MFNP (k) and the cross sectional compositional line profile (j). l-o) HAADF-STEM-EDS mapping images of an MFNP showing the yttrium K edge (l, yellow), yttrium L edge (m, green), iron K edge (n, orange), and gold K edge (o, blue). p) Photos of a PEG-coated MFNP sample in an aqueous solution under ambient light (left), exposed to a 980 nm laser (middle), and with a neighboring magnet (right). q) UV/Vis/NIR absorption spectra of MFNP nanocomposites prepared by adding different volumes of gold growth solutions. r) The corresponding UC luminescence spectra. s) Magnetization versus magnetic field plots for MFNPs, UCNP-IONP composite, and IONPs at room temperature. t) The T₂ relaxation rates (r₂) of PEG-MFNPs at different Fe concentrations. This figure is reprinted from [71]. Copyright 2011, Wiley-VCH Verlag GmbH & Co. KGaA.

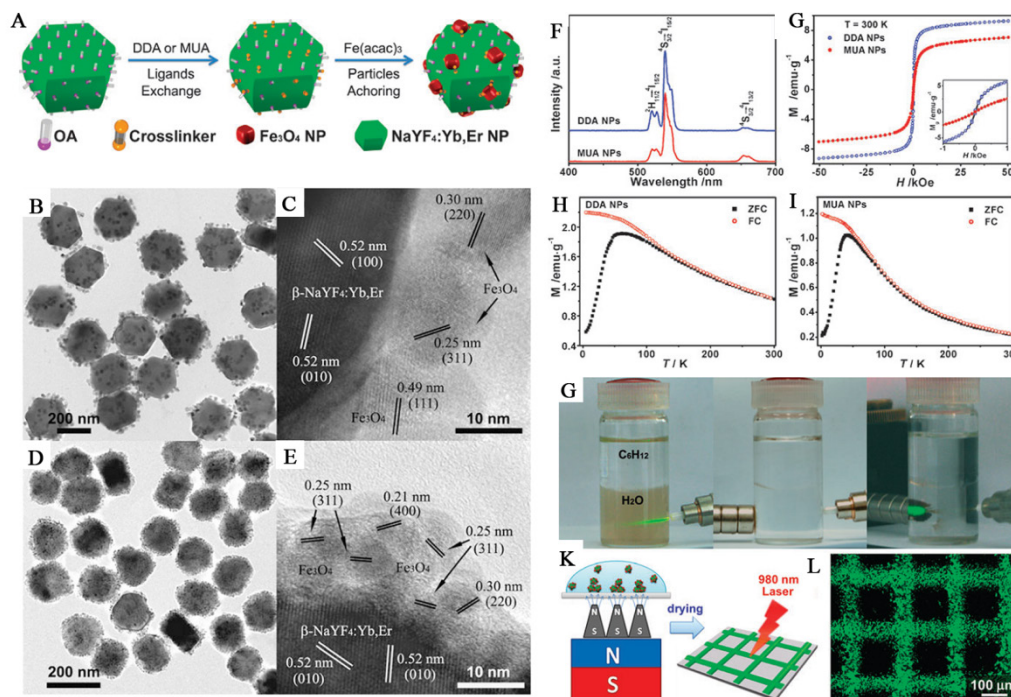


Figure 5. (A) Cross linker anchoring strategy for bi-functional $\text{Fe}_3\text{O}_4/\text{NaYF}_4:\text{Yb,Er}$ hetero-NPs. (B-E) TEM and HRTEM images of $\text{Fe}_3\text{O}_4/\text{NaYF}_4:\text{Yb,Er}$ hetero-NPs prepared with DDA (B, C) and MUA (D, E). (F-I) UC luminescent spectra (F) and field-dependent magnetization loops (G) of $\text{Fe}_3\text{O}_4/\text{NaYF}_4:\text{Yb,Er}$ hetero-NPs (inset, the magnified view of low field region), and ZFC/FC magnetization curves of hetero-NPs synthesized with DDA (H) and MUA (I), respectively. (G) Water-soluble $\text{Fe}_3\text{O}_4/\text{NaYF}_4:\text{Yb,Er}$ hetero-NPs after the ozonolysis treatment of surface OA ligands, and magnetic trapping of the NPs in water. (K) Scheme for magnetic patterning of the hydrophilic hetero-NPs. (L) The UC luminescent image of the pattern. This figure is reprinted from [72]. Copyright 2010, Royal Society of Chemistry.

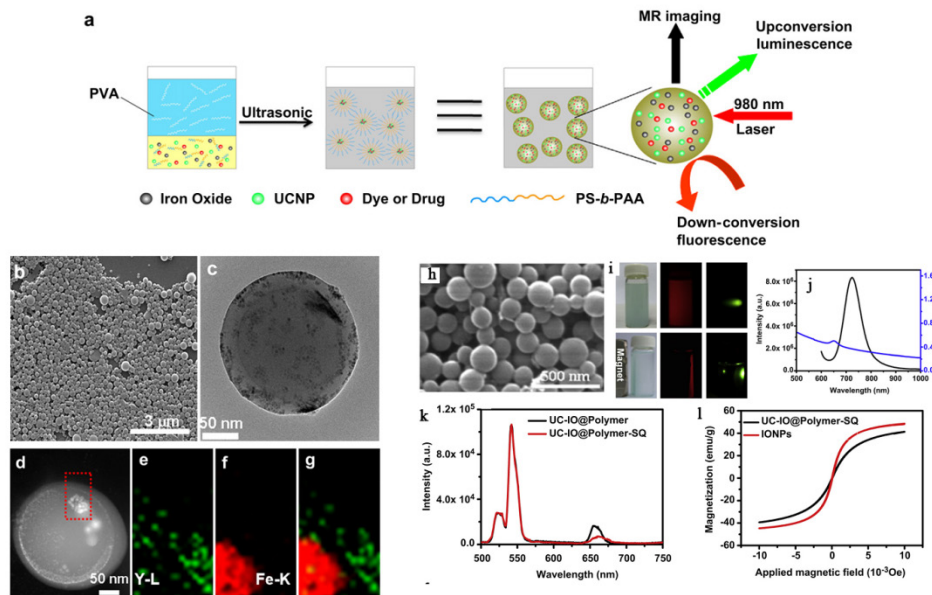


Figure 6. (a) A schematic illustration for UC-IO@Polymer nanocomposite synthesis and applications. (b) A representative SEM image of UC-IO@Polymer. The average particle size was around 200 nm (c) A TEM image of UC-IO@Polymer. (d-g) EDX mapping of the UC-IO@Polymer nanocomposite. (d) A high-angle annular dark-field scanning TEM (HAADF-STEM) image of a single UC-IO@Polymer nanoparticle. The area within the red rectangle was selected for EDS mapping. (e-g) HAADF-STEM-EDS mapping images of UC-IO@Polymer showing the yttrium L edge (e, green), iron K edge (f, red) and the merged image (g). (For interpretation of the references to colour in this figure legend, the reader is referred to the web version of this article.) (h) A SEM image of UC-IO@Polymer-SQ nanocomposite showing the average particle size of around 200 nm. (i) Photos of UC-IO@Polymer-SQ in aqueous solutions under the 980-nm laser and UV light with (upper) and without (down) the magnet. (j) UV/Vis and FL spectrum of UC-IO@Polymer-SQ nanocomposite. (k) UCL spectra of UC-IO@Polymer and UC-IO@Polymer-SQ. (l) Magnetization loops of IONPs and UC-IO@Polymer-SQ. This figure is reprinted from [74]. Copyright 2011, Elsevier B.V.

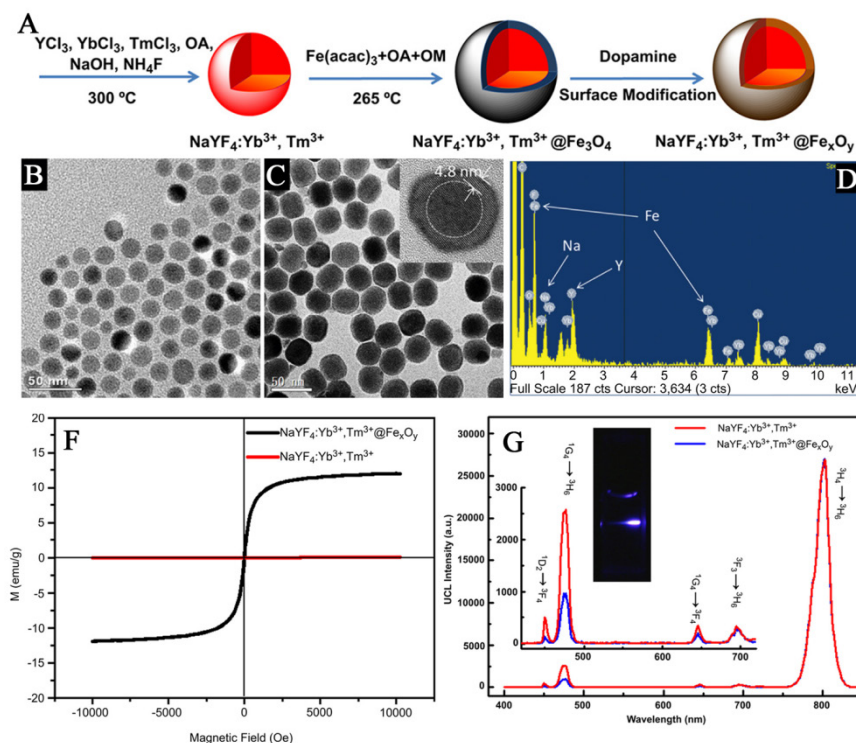


Figure 7. (A) Schematic representation of the synthetic routine of the water-soluble $\text{NaYF}_4:\text{Yb}^{3+}, \text{Tm}^{3+}@\text{Fe}_x\text{O}_y$ nanocrystals. (B, C) TEM image of $\text{NaYF}_4:\text{Yb}^{3+}, \text{Tm}^{3+}$ nanocrystals, $\text{NaYF}_4:\text{Yb}^{3+}, \text{Tm}^{3+}@\text{Fe}_3\text{O}_4$ nanocrystals. (D) EDX spectrum of the $\text{NaYF}_4:\text{Yb}^{3+}, \text{Tm}^{3+}@\text{Fe}_3\text{O}_4$ nanocrystals. (E) Magnetic hysteresis loops of measuring results of $\text{NaYF}_4:\text{Yb}^{3+}, \text{Tm}^{3+}$ (red line) and $\text{NaYF}_4:\text{Yb}^{3+}, \text{Tm}^{3+}@\text{Fe}_x\text{O}_y$ (black line) by vibrating sample magnetometer. (F) Room temperature UCL spectra of $\text{NaYF}_4:\text{Yb}^{3+}, \text{Tm}^{3+}$ (red line) and $\text{NaYF}_4:\text{Yb}^{3+}, \text{Tm}^{3+}@\text{Fe}_3\text{O}_4$ (blue line) under excitation at a CW 980 nm laser (power \geq 800 mW). This figure is reprinted from [75]. Copyright 2011, Elsevier B.V.

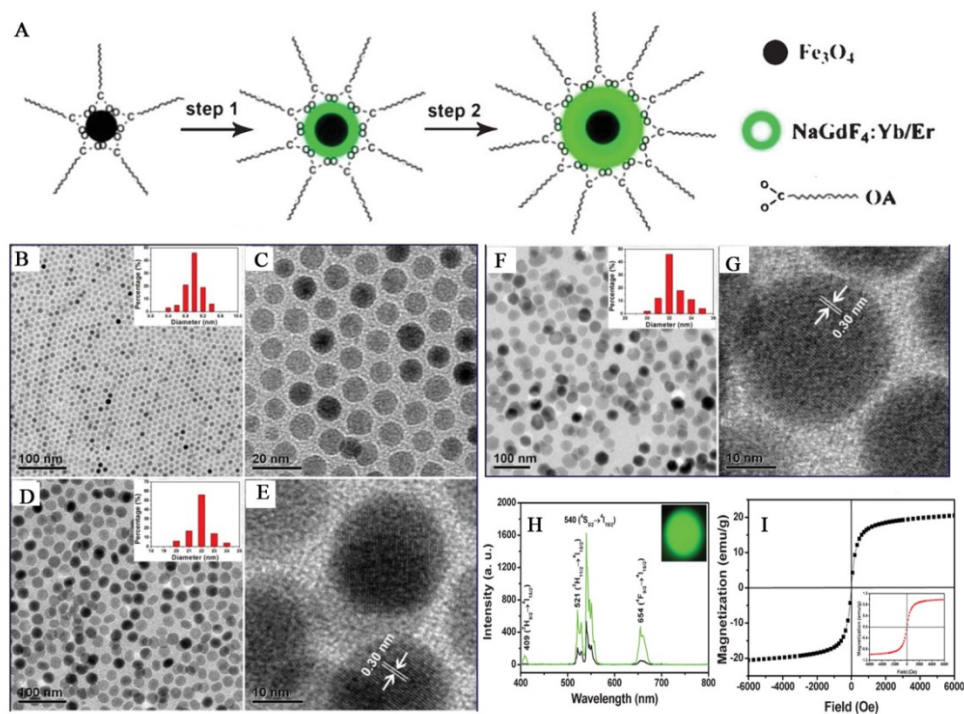


Figure 8. (A) Schematic formation processes of $\text{Fe}_3\text{O}_4@\text{NaGdF}_4:\text{Yb/Er}@\text{NaGdF}_4:\text{Yb/Er}$ NPs. (B) Low-resolution, (C) high-resolution TEM image of Fe_3O_4 NPs; (D) low-resolution, (E) high-resolution TEM images of $\text{Fe}_3\text{O}_4@\text{NaGdF}_4:\text{Yb/Er}$ NPs; (F) low-resolution, (G) high-resolution TEM images of $\text{Fe}_3\text{O}_4@\text{NaGdF}_4:\text{Yb/Er}@\text{NaGdF}_4:\text{Yb/Er}$ core-shell NPs. (H) Up-conversion emission spectra of $\text{Fe}_3\text{O}_4@\text{NaGdF}_4:\text{Yb/Er}$ (black line), $\text{Fe}_3\text{O}_4@\text{NaGdF}_4:\text{Yb/Er}@\text{NaGdF}_4:\text{Yb/Er}$ (green line) and the corresponding photograph under 980 nm irradiation (inset). (I) magnetizations of pure Fe_3O_4 and $\text{Fe}_3\text{O}_4@\text{NaGdF}_4:\text{Yb/Er}@\text{NaGdF}_4:\text{Yb/Er}$ NPs (inset) as a function of applied magnetic field measured at room temperature. This figure is reprinted from [76]. Copyright 2012, Royal Society of Chemistry.

3. Applications of Upconversion-Magnetic Nanoparticles

Zijlmans and co-workers were the first to exploit lanthanide-doped phosphors' upconverting properties to study biological recognition events [78]. Since then, there has been a substantial contribution to the development of biological labeling strategies that rely on the use of UC nanocrystals. Synthetic MNPs are emerging as versatile probes in biomedical applications, especially in the area of magnetic resonance imaging [79-84] and drug delivery [85-90]. So, when considering the applications of the upconversion-magnetic multifunctional nanoparticles, the strategies have been shown to be particularly attractive in multimodal imaging and magnetic targeted drug delivery. Most strategies developed in recent years can be divided into two categories: in vitro and in vivo applications.

3.1 Multimodal imaging

Organic fluorophores and fluorescent proteins have been traditionally used for in vivo imaging, but they typically suffer from low photostability and strong background auto fluorescence in the visible spectrum. Their broad emission bands often result in significant spectral overlapping, which can be a

problem in spectral interpretation during multicolor imaging. Quantum dots are more photostable than the organic fluorophores and have relatively narrow emission bandwidths. Their potential cytotoxicity over time, however, remains to be established. In contrast, high-quality UCNPs are investigated as fluorescent markers for imaging biological processes as well, as they benefit from the large anti-stokes shifts, narrow emission peaks, low toxicity, a high signal-to-noise ratio owing to the weak auto-fluorescence background generated by NIR excitation. However, photo luminescent imaging has one shortcoming of the low penetration depth of the excitation and emission light, which can be solved by magnetic resonance imaging (MRI). Owing to their large magnetic moment, superparamagnetic Fe_3O_4 nanoparticles have been combined with RE-UCNPs together for fabricating magnetic operation, T2-enhanced MR imaging and UCL imaging. For example, Liu et al. developed multifunctional nanoparticles (MFNPs), $\text{NaYF}_4:\text{Yb},\text{Er}@\text{Fe}_3\text{O}_4@\text{Au}$, which combined optical and magnetic properties useful for multimodality imaging (Figure 9 I) [71]. Recently, Li group also reported an imaging agent with $\text{NaYF}_4:\text{Yb},\text{Tm}@\text{Fe}_x\text{O}_y$ core/shell nanostructure for T2 MRI and UCL bimodal lymphatic imaging (Figure 9 II) [75].

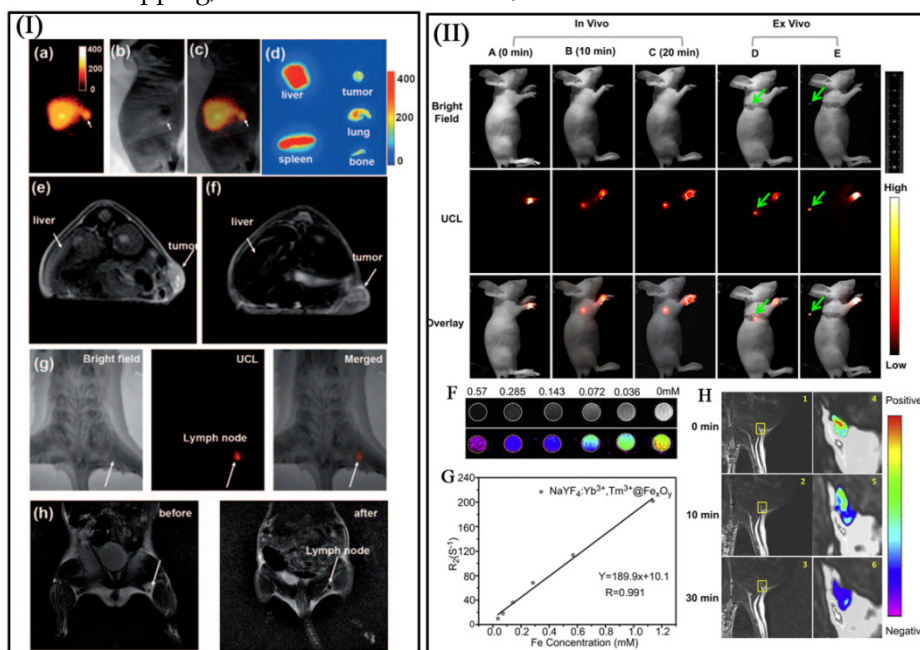


Figure 9. I a–c) The bright field (I a), UC luminescence (I b), and merged (I c) images of a KB tumor-bearing mouse one hour after intravenous injection of PEG–MFNPs. I d) Ex vivo UCL imaging showing accumulation of MNFPs in the liver, spleen, tumor, bone, and lung of the injected mouse at 24 h post injection. T2-weighted images of KB-tumor bearing nude mice with (I e) and without (I f) injection of MFNPs. Multimodal UCL (I g) and MR (I h) imaging for in vivo lymphangiography mapping using MFNPs [71]. In vivo UCL imaging of lymphatic system after injection with $\text{NaYF}_4:\text{Yb}^{3+},\text{Tm}^{3+}@FexO_y$ nanocrystals into a nude mouse at various time (II A) 0 min, (II B) 10 min and (II C) 20 min. (II F) T2-weighted and color-mapped MR images of various molar concentrations of $\text{NaYF}_4:\text{Yb}^{3+},\text{Tm}^{3+}@FexO_y$ nanocrystals. Deionized water (0 mg/mL) was the reference. (II G) Relaxation rate R_2 ($1/T_2$) vs. various molar concentrations of hydrophilic $\text{NaYF}_4:\text{Yb}^{3+},\text{Tm}^{3+}@FexO_y$ nanocrystals at room temperature using a 3T MRI scanner. (II H) MR images of the armpit region after injection with $\text{NaYF}_4:\text{Yb}^{3+},\text{Tm}^{3+}@FexO_y$ nanocrystals and Color-mapped coronal images of lymph node at various time [75]. This figure is reprinted from [71] and [75]. Copyright 2011 Wiley-VCH Verlag GmbH & Co. KGaA and 2011 Elsevier B.V.

By introducing the high UC luminescence quantum yield NaLuF₄ as luminescent shell, Li group designed and synthesized the core/shell upconversion-magnetic Fe₃O₄@NaLuF₄:Yb,Er/Tm nanostructure (Figure 10 D-F) [67]. Owing to the large atomic number and high X-ray absorption coefficient of lutetium, NaLuF₄ can be used as a contrast agent for CT imaging. The UC luminescent, magnetic and X-ray attenuation properties of these nanoparticles were

investigated in detail. Moreover, they also investigated the multimodal performance for MR, CT and UCL imaging. Xu and co-workers also demonstrate a facial synthetic method to prepare a novel UC-IO@Polymer-SQ nanocomposite for multi-model imaging. It can be used for triple-modal UCL/down-conversion FL/MR imaging in vitro and in vivo (Figure 10 A-C) [74].

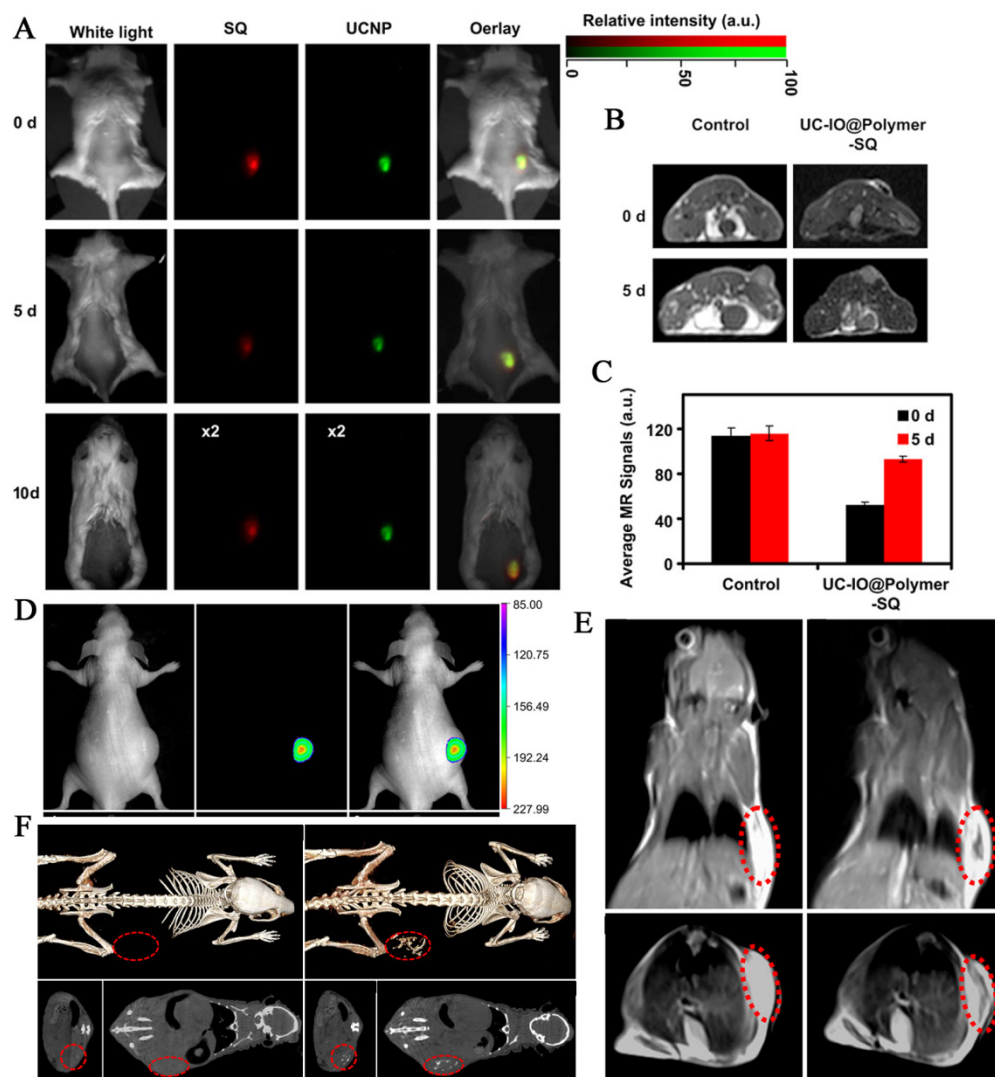


Figure 10. (A) FL/UCL images of mice subcutaneously injected with UC-IO@Polymer-SQ labeled 4T1 cells taken 0 day, 5 days and 10 days after injection. (B) T2-weighted MR images of mice inoculated with UC-IO@Polymer-SQ labeled 4T1 cells and control unlabeled cells after 0 day and 5 days. (C) The MR signals plot of tumors on mice inoculated with UC-IO@Polymer-SQ treated 4T1 cells and untreated cells after 0 day and 5 days [74]. (D) In vivo UCL images of the tumor-bearing nude mice in bright field, dark field and overlay images after intratumoral injection of MUCNP. (E) T2-weighted coronal and transversal cross-sectional images of the nude mice bearing a tumor pre-injection and at 30 min after intratumoral injection of MUCNP. (F) In vivo CT volume-rendered and maximum intensity projection of coronal, transversal images of the tumor-bearing mouse after intratumoral injection [67]. This figure is reprinted from [67] and [74]. Copyright 2011 and 2012 Elsevier B.V.

3.2 Magnetic targeted drug delivery

One major problem in current chemotherapy is the drug dosage given to patients. A low dosage of drug is ineffective in the treatment of a tumor, whereas a high dosage of chemo-therapeutics is intolerable for patients due to toxicity and side effects. Therefore a new design for anticancer drugs is desirable to increase the local effective therapeutic concentration. Along this line, combine MNPs with the pharmaceutical carriers, conspired with UC luminescent nanoparticles as bio-labeling, the upconversion-magnetic multifunctional nanoparticles is considered to be one of the most effective ways to increase the therapeutic effectiveness.

Most recently, our group reported a concentric nanostructure with both UC and magnetic properties (Figure I) [66]. Importantly, the nanoparticle additionally contains a hollow volume that can accommodate a drug payload. The material was used as a drug delivery system to load the anti-cancer drug.

Cytotoxicity and cell imaging experiments demonstrate the nanorattle materials to be biocompatible and easily endocytosed by cells. Intracellular drug release was also observed. The multifunctional nanorattles show advantages for in vivo enhancement of therapy efficacy by reducing the systemic toxicity of anti tumor drugs both through protection of the drug during circulation and by using magnetic fields to target the material to the lesion. Furthermore, with such a coreshell architecture surface coatings tailored for tumor targeting are conceivable, making it possible to engineer additional functionalities into this nanosystem. Except the triple-modal imaging of the polymer encapsulated UCNPs-iron oxide nanocomposites, which was developed by the Liu group, a chemotherapy drug, doxorubicin, is also loaded into the nanocomposite, forming an UC-IO@Polymer-DOX complex, which enables novel imaging-guided and magnetic targeted drug delivery (Figure 11 II) [74].

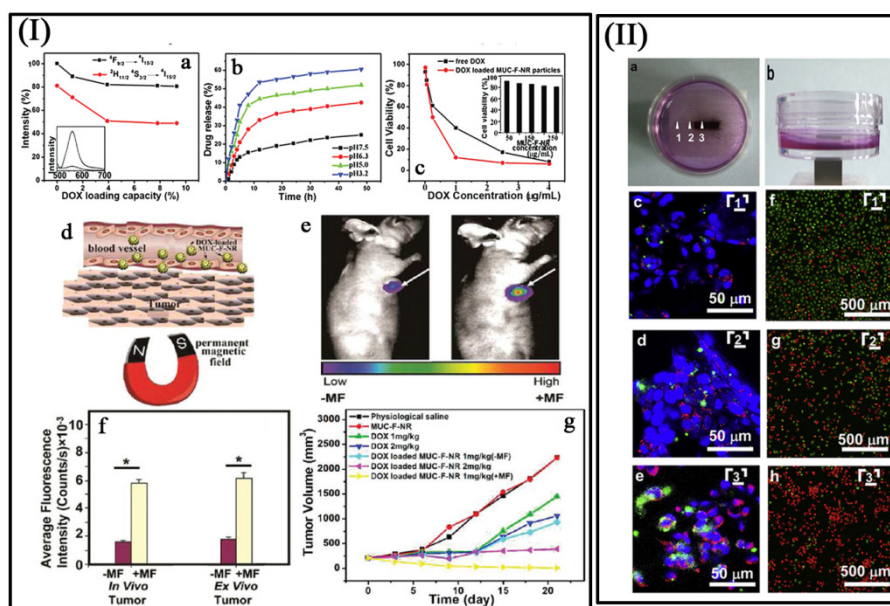


Figure 11. (I a) Integrated green and red UC emission intensity as a function of the DOX loading capacity; inset is the fluorescence spectra of free DOX and DOX loaded MUC-F-NR. (I b) pH-dependent release kinetics of DOX from loaded MUC-F-NR. (I c) Cell viability data of QGY-7701 cells incubated with free DOX and DOX-loaded MUC-F-NR at different concentrations; inset is cell viability with concentrations of drug free MUC-F-NR from 50 to 250 $\mu\text{g/mL}$ for 72 h. (I d) Schematic illustration of targeting of DOX loaded multifunctional drug carrier to tumor cells assisted by an externally applied magnetic field (MF). (I e) Tumor location as defined by MUC-F-NR intensity increases with 1 h magnetic field treatment. (I f) The luminescence signal was measured from the whole tumor in vivo and ex vivo. (Excitation was provided by the CW infrared laser at 980 nm and UC luminescence signals were collected at 650 (10 nm. Fluence rates for 980 nm excitation light were 80 mW/cm².) (I g) Tumor volume changes of saline-treated mice compared to mice treated with MUC-F-NR, DOX, and DOX loaded MUC-F-NR over 21 d in the absence and presence of magnetic field [66]. (II a, b) Photos of the cell culture dish with a magnet placed under the center of the dish. (II c - II e) Confocal UC luminescence and fluorescence images of HeLa cells after being incubated with UC-IO@Polymer-DOX in the presence of a magnetic field. (II f - II h) Confocal fluorescence images of calcein AM (green, live cells) and PI (red, dead cells) co-stained cells after magnetic targeted drug delivery [74]. This figure is reprinted from [66] and [74]. Copyright 2012 American Chemical Society and 2011 Elsevier B.V.

4. Conclusions and Outlook

This review has described recent developments in the synthesis and applications of upconversion-magnetic multifunctional nanoparticles. This research continues to be a vibrant and growing interdisciplinary field. In the near future, there are a number of areas of research that are particularly promising, but concerted efforts are still required for success:

- It was found that the methods for the synthesis of the upconversion-magnetic multifunctional nanoparticles are all the multi-step process. So, on the basis of the guarantee of high photoluminescence efficiency optical property and strong magnetic property, it is particularly important to develop a more simple protocol (*e.g.* one-pot method) to obtain the hybrid materials.
- Although there are many attractive advantages compared with the organic fluorophores and QDs, the efficiency of the UCNPs are still very low, which will further influence the performance and applications of the upconversion-magnetic multifunctional nanoparticles.

Despite the fact that some successful results were obtained, the development of multifunctional nanoprobe for multimodal imaging is still in its early stages. It is still a major challenge to design a multifunctional nanoprobe for simultaneous bio-imaging covering optical imaging, MRI, CT and other kinds of monitoring. In addition, active targeted multimodal imaging and drug delivery system still needs to be developed to realize the disease detection and therapy simultaneously.

Competing Interests

The authors have declared that no competing interest exists.

References

1. Auzel F. Upconversion and Anti-Stokes Processes with f and d Ions in Solids. *Chem Rev.* 2004; 104: 139-74.
2. Gamelin DR, Gudiel HU. Design of luminescent inorganic materials: new photophysical processes studied by optical spectroscopy. *Acc Chem Res.* 2000; 33: 235-42.
3. Wang F, Liu XG. Recent advances in the chemistry of lanthanide-doped upconversion nanocrystals. *Chem Soc Rev.* 2009; 38: 976-89.
4. Haase M, Schafer H. Upconverting Nanoparticles. *Angew Chem Int Ed.* 2011; 50: 5808-29.
5. Zhou J, Liu Z, Li F. Upconversion nanophosphors for small-animal imaging. *Chem Soc Rev.* 2012; 41: 1323-49.
6. Auzel F. Materials and devices using double-pumped phosphors with energy transfer. *Proc IEEE.* 1973; 61: 758-86.
7. Chivian JS, Case WE, Infern DD. The photon avalanche: A new phenomenon in Pr³⁺-based infrared quantum counters. *Appl Phys Lett.* 1979; 35: 124.
8. Zhang F, Braun GB, Shi YF, Zhang YC, Sun XH, Reich NO, Zhao D, Stucky G. Fabrication of Ag@SiO₂@Y₂O₃:Er Nanostructures for Bioim-

aging; Tuning of the Upconversion Fluorescence with Silver Nanoparticles. *J Am Chem Soc.* 2010; 132: 2850-51.

9. Jin J, Gu YJ, Man CWY, Cheng J, Xu Z, Zhang Y, Wang H, Lee VHY, Cheng SH, Wong WT. Polymer-Coated NaYF₄:Yb³⁺,Er³⁺ Upconversion Nanoparticles for Charge-Dependent Cellular Imaging. *ACS Nano.* 2011; 5: 7838-47.
10. Liu Q, Sun Y, Yang T, Feng W, Li C, Li F. Sub-10 nm Hexagonal Lanthanide-Doped NaLuF₄ Upconversion Nanocrystals for Sensitive Bioimaging in Vivo. *J Am Chem Soc.* 2011; 133: 17122-5.
11. Zhang F, Haushalter RC, Haushalter RW, Shi Y, Zhang Y, Ding K, Zhao D, Stucky G. Rare-Earth Upconverting Nanobarcodes for Multiplexed Biological Detection. *Small.* 2011; 7: 1972-6.
12. Dai Y, Ma P, Cheng Z, Kang X, Zhang X, Hou Z, Li C, Yang D, Zhai X, Lin J. Up-Conversion Cell Imaging and pH-Induced Thermally Controlled Drug Release from NaYF₄:Yb³⁺/Er³⁺@Hydrogel Core-Shell Hybrid Microspheres. *ACS Nano.* 2012; 6: 3327-38.
13. Chen ZG, Chen HL, Hu H, Yu MX, Li FY, Zhang Q, Zhou ZG, Yi T, Huang CH. Versatile Synthesis Strategy for Carboxylic Acid functionalized Upconverting Nanophosphors as Biological Labels. *J Am Chem Soc.* 2008; 130: 3023-9.
14. Ostrowski AD, Chan EM, Gargas DJ, Katz EM, Han G, Schuck PJ, Milliron DJ, Cohen BE. Controlled Synthesis and Single-Particle Imaging of Bright, Sub-10 nm Lanthanide-Doped Upconverting Nanocrystals. *ACS Nano.* 2012; 6: 2686-92.
15. Bogdan N, Vetrone F, Ozin GA, Capobianco JA. Synthesis of Ligand-Free Colloidally Stable Water Dispersible Brightly Luminescent Lanthanide-Doped Upconverting Nanoparticles. *Nano Lett.* 2011; 11: 835-40.
16. Qian HS, Guo HC, Ho PC, Mahendran R, Zhang Y. Mesoporous-Silica-Coated Up-Conversion Fluorescent Nanoparticles for Photodynamic Therapy. *Small.* 2009; 5: 2285-90.
17. Zhang F, Shi Q, Zhang Y, Shi Y, Ding K, Zhao D, Stucky G. Fluorescence Upconversion Microbarcodes for Multiplexed Biological Detection: Nucleic Acid Encoding. *Adv Mater.* 2011; 23: 3775-9.
18. Xu CT, Svenmarker P, Liu H, Wu X, Messing ME, Wallenberg LR, Engels SA. High-Resolution Fluorescence Diffuse Optical Tomography Developed with Nonlinear Upconverting Nanoparticles. *ACS Nano.* 2012; 6: 4788-95.
19. Stouwdam JW, van Veggel FCJM. Near-infrared emission of redispersible Er³⁺, Nd³⁺, and Ho³⁺ doped LaF₃ nanoparticles. *Nano Letters* 2002; 2: 733-7.
20. Yi GS, Chow GM. Colloidal LaF₃:Yb,Er, LaF₃:Yb,Ho and LaF₃:Yb,Tm nanocrystals with multicolor upconversion fluorescence. *J Mater Chem.* 2005; 15: 4460-4.
21. Wei Y, Lu FQ, Zhang XR, Chen D. Polyol-mediated synthesis and luminescence of lanthanide-doped NaYF₄ nanocrystal upconversion phosphors. *J Alloys Compd.* 2008; 455: 376-84.
22. Wang L, Li Y. Controlled Synthesis and Luminescence of Lanthanide Doped NaYF₄ Nanocrystals. *Chem Mater.* 2007; 19: 727-34.
23. Zhang F, Wan Y, Yu T, Zhang F, Shi Y, Xie S, Li Y, Xu L, Tu B, Zhao D. Uniform Nanostructured Arrays of Sodium Rare-Earth Fluorides for Highly Efficient Multicolor Upconversion Luminescence. *Angew Chem Int. Ed.* 2007; 46: 7976-9.
24. Liu C, Chen D. Controlled synthesis of hexagon shaped lanthanide-doped LaF₃ nanoplates with multicolor upconversion fluorescence. *J Mater Chem.* 2007; 17: 3875-80.
25. Patra A, Friend CS, Kapoor R, Prasad PN. Fluorescence upconversion properties of Er³⁺-doped TiO₂ and BaTiO₃ nanocrystallites. *Chem Mater.* 2003; 15: 3650-5.
26. Venkatramu V, Falcomer D, Speghini A, Bettinelli M, Jayasankar CK. Synthesis and Luminescence Properties of Er³⁺-doped Lu₃Ga₅O₁₂ Nanocrystals. *J Lumin.* 2008; 128: 811-3.
27. Zhang Y, Sun X, Si R, You L, Yan C. Single-Crystalline and Monodisperse LaF₃ Triangular Nanoplates from a Single-Source Precursor. *J Am Chem Soc.* 2005; 127: 3260-1.
28. Vetrone F, Boyer JC, Capobianco JA, Speghini A, Bettinelli M. Significance of Yb³⁺ concentration on the upconversion mechanisms in codoped Y₂O₃:Er³⁺, Yb³⁺ nanocrystals. *J Appl Phys.* 2004; 96: 661-7.
29. Luo X, Cao W. Ethanol-assisted solution combustion method to prepare La₂O₃:Yb,Pr nanometer phosphor. *J Alloys Compd.* 2008; 460: 529-34.
30. Xu L, Yu Y, Li X, Somsaleang G, Zhang Y, Gao H, Zhang Z. Synthesis and upconversion properties of monoclinic Gd₂O₃:Er³⁺ nanocrystals. *Opt Mater.* 2008; 30: 1284-8.
31. Hu F, Wei L, Zhou Z, Ran Y, Li Z, Gao M. Preparation of Biocompatible Magnetite Nanocrystals for In Vivo Magnetic Resonance Detection of Cancer. *Adv Mater.* 2006; 18: 2553-6.
32. Chen FH, Zhang LM, Chen QT, Zhang Y, Zhang ZJ. Synthesis of a novel magnetic drug delivery system composed of doxorubicin-conjugated

- Fe₃O₄ nanoparticle cores and a PEG-functionalized porous silica shell. *Chem Commun.* 2010; 46: 8633-5.
33. Yu MK, Jeong YY, Park J, Park S, Kim JW, Min JJ, Kim K, Jon S. Drug-Loaded Superparamagnetic Iron Oxide Nanoparticles for Combined Cancer Imaging and Therapy In Vivo. *Angew Chem Int Ed.* 2008; 47: 5362-5.
34. Jun Y, Huh YM, Choi J, Lee JH, Song HT, Kim S, Yoon S, Kim KS, Shin JS, Suh JS, Cheon J. Nanoscale Size Effect of Magnetic Nanocrystals and Their Utilization for Cancer Diagnosis via Magnetic Resonance Imaging. *J Am Chem Soc.* 2005; 127: 5732-3.
35. Huh YM, Jun Y, Song HT, Kim S, Choi J, Lee JH, Yoon S, Kim KS, Shin JS, Suh JS, Cheon J. In Vivo Magnetic Resonance Detection of Cancer by Using Multifunctional Magnetic Nanocrystals. *J Am Chem Soc.* 2005; 127:12387-91.
36. Katagiri K, Imai Y, Koumoto K, Kaiden T, Kono K, Aoshima S. Magneto-responsive On-Demand Release of Hybrid Liposomes Formed from Fe₃O₄ Nanoparticles and Thermosensitive Block Copolymers. *Small.* 2011; 7: 1683-9.
37. Chen H, Deng C, Zhang X. Synthesis of Fe₃O₄@SiO₂@PMMA Core-Shell-Shell Magnetic Microspheres for Highly Efficient Enrichment of Peptides and Proteins for MALDI-ToF MS Analysis. *Angew Chem Int Ed.* 2010; 49: 607-11.
38. Seo WS, Lee JH, Sun X, Suzuki Y, Mann D, Liu Z, Terashima M, Yang PC, McConnell MV, Nishimura DG, Dai H. FeCo/graphitic-shell nanocrystals as advanced magnetic-resonance- imaging and near-infrared agents. *Nat Mater.* 2006; 5: 971-6.
39. Nasongkla N, Bey E, Ren J, Ai H, Khemtong C, Guthi JS, Chin SF, Sherry AD, Boothman DA, Gao J. Multifunctional Polymeric Micelles as Cancer-Targeted, MRI-Ultrahigh Sensitive Drug Delivery Systems. *Nano Lett.* 2006; 6: 2427-30.
40. Song HT, Choi J, Huh YM, Kim S, Jun Y, Suh JS, Cheon J. Surface Modulation of Magnetic Nanocrystals in the Development of Highly Efficient Magnetic Resonance Probes for Intracellular Labeling. *J Am Chem Soc.* 2005; 127: 9992-3.
41. Jun Y, Lee JH, Cheon J. Chemical Design of Nanoparticle Probes for High- Performance Magnetic Resonance Imaging. *Angew Chem Int Ed.* 2008; 47: 5122-35.
42. Hou Y, Xu Z, Sun S. Controlled Synthesis and Chemical Conversions of FeO Nanoparticles. *Angew Chem Int Ed.* 2007; 46: 6329-32.
43. Xu Z, Shen C, Hou Y, Gao H, Sun S. Oleylamine as Both Reducing Agent and Stabilizer in a Facile Synthesis of Magnetite Nanoparticles. *Chem Mater.* 2009; 21: 1778-80.
44. Tan Y, Zhuang Z, Peng Q, Li Y. Room-Temperature Soft Magnetic Iron Oxide Nanocrystals: Synthesis, Characterization, and Size-Dependent Magnetic Properties. *Chem Mater.* 2008; 20: 5029-34.
45. Li X, Si H, Niu JZ, Shen H, Zhou C, Yuan H, Wang H, Ma L, Li LS. Size-controlled syntheses and hydrophilic surface modification of Fe₃O₄, Ag, and Fe₃O₄/Ag heterodimer nanocrystals. *Dalton Trans.* 2010; 39: 10984-9.
46. Sun S, Zeng H, Robinson DB, Raoux S, Rice PM, Wang SX, Li G. Monodisperse MFe₂O₄ (M Fe, Co, Mn) Nanoparticles. *J Am Chem Soc.* 2004; 126: 273-9.
47. Kim D, Lee N, Park M, Kim BH, An K, Hyeon T. Synthesis of Uniform Ferrimagnetic Magnetite Nanocubes. *J Am Chem Soc.* 2009; 131: 454-5.
48. Kovalenko MK, Bodnarchuk MI, Lechner RT, Hesser G, Schaffler F, Heiss W. Fatty Acid Salts as Stabilizers in Size- and Shape-Controlled Nanocrystal Synthesis: The Case of Inverse Spinel Iron Oxide. *J Am Chem Soc.* 2007; 129: 6352-3.
49. Sun S, Zeng H. Size-Controlled Synthesis of Magnetite Nanoparticles. *J Am Chem Soc.* 2002; 124: 8204-5.
50. Park J, An K, Hwang Y, Park JG, Noh HJ, Kim JY, Park JH, Hwang NM, Hyeon T. Ultra-large-scale syntheses of monodisperse nanocrystals. *Nature Materials* 2004; 3: 891-5.
51. Nagasubramanian R, Innocent F, Ratain MJ. Pharmacogenetics in cancer treatment. *Annu Rev Med.* 2003; 54: 437-52.
52. Allen TM, Cullis PR. Drug Delivery Systems: Entering the Mainstream. *Science.* 2004; 303: 1818-22.
53. Janib SM, Moses AS, MacKay JA. Imaging and drug delivery using theranostic nanoparticles. *Adv Drug Delivery Rev.* 2010; 62: 1052-63.
54. van Vlerken LE, Duan Z, Seiden MV, Amiji MM. Modulation of intracellular ceramide using polymeric nanoparticles to overcome multidrug resistance in cancer. *Cancer Res.* 2007; 67: 484350.
55. Kim JY, Park SG, Lee JE, Jin SM, Lee JH, Lee IS, Yang IL, Kim JS, Kim SK, Cho MH, Hyeon TH. Designed Fabrication of Multifunctional Magnetic Gold Nanoshells and Their Applications to Immunotargeted Magnetic Resonance Imaging and Rapid Noninvasive Photothermal Therapy. *Angew Chem Int Ed.* 2006; 45: 7754-8.
56. Selvan ST, Patra PK, Ang CY, Ying JY. Synthesis of Silica-Coated Semiconductor and Magnetic Quantum Dots and Their Use in the Imaging of Live Cells. *Angew Chem Int Ed.* 2007; 46: 2448-52.
57. Lim SJ, An BK, Jung SD, Chung MA, Park SY. Photoswitchable Organic Nanoparticles and a Polymer Film Employing Multifunctional Molecules with Enhanced Fluorescence Emission and Bistable Photochromism. *Angew Chem Int Ed.* 2004; 43: 6346-50.
58. Kim JY, Kim HS, Lee N, Kim T, Kim H, Yu T, Song IC, Moon WK, Hyeon TH. Multifunctional Uniform Nanoparticles Composed of a Magnetite Nanocrystal Core and a Mesoporous Silica Shell for Magnetic Resonance and Fluorescence Imaging and for Drug Delivery. *Angew Chem Int Ed.* 2008; 47: 8438-41.
59. Salgueirino-Maceira V, Correa-Duarte MA, Spasova M, Liz-Marzan LM, Farle M. Composite Silica Spheres with Magnetic and Luminescent Functionalities. *Adv Func Mater.* 2006; 16: 509-14.
60. Insin N, Tracy JB, Lee H, Zimmer JP, Westervelt RM, Bawendi MG. Incorporation of iron oxide nanoparticles and quantum dots into silica microspheres. *ACS Nano* 2008; 2: 197-202.
61. Li ZQ, Zhang Y, Jiang S. Multicolor Core/Shell-Structured Upconversion Fluorescent Nanoparticles. *Adv Mater.* 2008; 20: 4765-8.
62. van de Rijke F, Zijlmans H, Li S, Vail T, Raap AK, Niedbala RS, Tanke HJ. Up-converting phosphor reporters for nucleic acid microarrays. *Nat Biotechnol.* 2001; 19: 273-6.
63. Wang F, Liu XG. Recent advances in the chemistry of lanthanide-doped upconversion nanocrystals. *Chem Soc Rev.* 2009; 38: 976-89.
64. Auzel F. Upconversion and Anti-Stokes Processes with f and d Ions in Solids. *Chem Rev.* 2004; 104: 139-74.
65. Mai HX, Zhang YW, Si R, Yan ZG, Yan CH. High-Quality Sodium Rare-Earth Fluoride Nanocrystals: Controlled Synthesis and Optical Properties. *J Am Chem Soc.* 2006; 128: 6426-36.
66. Zhang F, Braun GB, Pallaoro A, Zhang Y, Shi Y, Cui D, Moskovits M, Zhao D, Stucky GD. Mesoporous Multifunctional Upconversion Luminescent and Magnetic "Nanorattle" Materials for Targeted Chemotherapy. *Nano Letters.* 2012; 12: 61-7.
67. Zhu X, Zhou J, Chen M, Shi M, Feng W, Li F. Core-shell Fe₃O₄@NaLuF₄:Yb,Er/Tm nanostructure for MRI, CT and upconversion luminescence tri-modality imaging. *Biomaterials.* 2012; 33: 4618-27.
68. Liu Z, Yi G, Zhang H, Ding J, Zhang Y, Xue J. Monodisperse silica nanoparticles encapsulating upconversion fluorescent and superparamagnetic nanocrystals. *Chem Commun.* 2008; 694-6.
69. Mi C, Zhang J, Gao H, Wu X, Wang M, Wu Y, Di Y, Xu Z, Mao C, Xu S. Multifunctional nanocomposites of superparamagnetic (Fe₃O₄) and NIR-responsive rare earth-doped up-conversion fluorescent (NaYF₄:Yb,Er) nanoparticles and their applications in biolabeling and fluorescent imaging of cancer cells. *Nanoscale.* 2010; 2: 1141-8.
70. Hu D, Chen M, Gao Y, Li F, Wu L. A facile method to synthesize superparamagnetic and up-conversion luminescent NaYF₄:Yb,Er/Tm@SiO₂@Fe₃O₄ nanocomposite particles and their bioapplication. *J Mater Chem.* 2011; 21: 11276-82.
71. Cheng L, Yang K, Li Y, Chen J, Wang C, Shao M, Lee S, Liu Z. Facile Preparation of Multifunctional Upconversion Nanoprobes for Multimodal Imaging and Dual-Targeted Photothermal Therapy. *Angew Chem Int Ed.* 2011; 50: 7385-90.
72. Shen J, Sun LD, Zhang YW, Yan CH. Superparamagnetic and upconversion emitting Fe₃O₄/NaYF₄:Yb,Er hetero-nanoparticles via a crosslinker anchoring strategy. *Chem Commun.* 2010; 46: 5731-3.
73. Cheng L, Yang K, Li Y, Zeng X, Shao M, Lee S, Liu Z. Multifunctional nanoparticles for upconversion luminescence/MR multimodal imaging and magnetically targeted photothermal therapy. *Biomaterials.* 2012; 33: 2215-22.
74. Xu H, Cheng L, Wang C, Ma X, Li Y, Liu Z. Polymer encapsulated up-conversion nanoparticle/iron oxide nanocomposites for multimodal imaging and magnetic targeted drug delivery. *Biomaterials.* 2011; 32: 9364-73.
75. Xia A, Gao Y, Zhou J, Li C, Yang T, Wu D, Wu L, Li F. Core-shell NaYF₄:Yb³⁺,Tm³⁺@Fe₃O₄ nanocrystals for dual-modality T₂-enhanced magnetic resonance and NIR-to-NIR upconversion luminescent imaging of small-animal lymphatic node. *Biomaterials.* 2011; 32: 7200-8.
76. Zhong C, Yang P, Li X, Li C, Wang D, Gai S, Lin J. Monodisperse bifunctional Fe₃O₄@NaGdF₄:Yb/Er@NaGdF₄:Yb/Er core-shell nanoparticles. *RSC Advances.* 2012; 2: 3194-7.
77. Zhang M, Shi S, Meng J, Wang X, Fan H, Zhu Y, Wang X, Qian Y. Preparation and Characterization of Near-Infrared Luminescent Bifunctional Core/Shell Nanocomposites. *J Phys Chem C.* 2008; 112: 2825-30.
78. Zijlmans HJ, Bonnet J, Burton J, Kardos K, Vail T, Niedbala RS, Tanke HJ. Detection of cell and tissue surface antigens using up-converting phosphors: a new reporter technology. *Anal Biochem.* 1999; 267: 30-6.

79. Fan HM, Olivo M, Shuter B, Yi JB, Bhuvanewari R, Tan HR, Xing GC, Ng CT, Liu L, Lucky SS, Bay BH, Ding J. Quantum Dot Capped Magnetite Nanorings as High Performance Nanoprobe for Multiphoton Fluorescence and Magnetic Resonance Imaging. *J Am Chem Soc.* 2010; 132: 14803-11.
80. Cheong S, Ferguson P, Feindel KW, Hermans IF, Callaghan PT, Meyer C, Slocombe A, Su CH, Cheng FY, Yeh CS, Ingham B, Toney MF, Tilley RD. Simple Synthesis and Functionalization of Iron Nanoparticles for Magnetic Resonance Imaging. *Angew Chem Int Ed.* 2011; 50: 4206-09.
81. Malvindi MA, Greco A, Conversano F, Figuerola A, Corti M, Bonora M, Lascialfari A, Doumari HA, Moscardini M, Cingolani R, Gigli G, Casciaro S, Pellegrino T, Ragusa A. Magnetic/Silica Nanocomposites as Dual-Mode Contrast Agents for Combined Magnetic Resonance Imaging and Ultrasonography. *Adv Funct Mater.* 2011; 21: 2548-55.
82. Li Z, Yi PW, Sun Q, Lei H, Zhao HL, Zhu ZH, Smith SC, Lan MB, Lu GQ. Ultrasmall Water-Soluble and Biocompatible Magnetic Iron Oxide Nanoparticles as Positive and Negative Dual Contrast Agents. *Adv Funct Mater.* 2012; 22: 2387-93.
83. Tian Y, Yu B, Li X, Li K. Facile solvothermal synthesis of monodisperse Fe₃O₄ nanocrystals with precise size control of one nanometre as potential MRI contrast agents. *J Mater Chem.* 2011; 21: 2476-81.
84. Hu F, MacRenaris KW, Waters EA, Liang T, Schultz-Sikma EA, Eckermann AL, Meade TJ. Ultrasmall, Water-Soluble Magnetite Nanoparticles with High Relaxivity for Magnetic Resonance Imaging. *J Phys Chem C.* 2009; 113: 20855-60.
85. Lee JE, Lee N, Kim H, Kim J, Choi SH, Kim JH, Kim T, Song IC, Park SP, Moon WK, Hyeon T. Uniform Mesoporous Dye-Doped Silica Nanoparticles Decorated with Multiple Magnetite Nanocrystals for Simultaneous Enhanced Magnetic Resonance Imaging, Fluorescence Imaging, and Drug Delivery. *J Am Chem Soc.* 2010; 132: 552-7.
86. Wu H, Zhang S, Zhang J, Liu G, Shi J, Zhang L, Cui X, Ruan M, He Q, Bu W. A Hollow-Core, Magnetic, and Mesoporous Double-Shell Nanostructure: In Situ Decomposition/Reduction Synthesis, Bioimaging, and Drug-Delivery Properties. *Adv Funct Mater.* 2011; 21: 1850-62.
87. Gong X, Peng S, Wen W, Sheng P, Li W. Design and Fabrication of Magnetically Functionalized Core/Shell Microspheres for Smart Drug Delivery. *Adv Funct Mater.* 2009; 19: 292-7.
88. Chen FH, Zhang LM, Chen QT, Zhang Y, Zhang ZJ. Synthesis of a novel magnetic drug delivery system composed of doxorubicin-conjugated Fe₃O₄ nanoparticle cores and a PEG-functionalized porous silica shell. *Chem Commun.* 2010; 46: 8633-5.
89. Zhang XF, Mansouri S, Clime L, Ly HQ, Yahia LH, Veres T. Fe₃O₄-silica core-shell nanoporous particles for high-capacity pH-triggered drug delivery. *J Mater Chem.* 2012; 22: 14450-7.
90. Santra S, Kaittanis C, Grimm J, Perez JM. Drug/Dye-Loaded, Multifunctional Iron Oxide Nanoparticles for Combined Targeted Cancer Therapy and Dual Optical/Magnetic Resonance Imaging. *Small.* 2009; 5: 1862-8.